JOURNAL OF COMPUTATIONAL PHYSICS 56, 272–286 (1984)

Discrete Orthogonal Function Expansions for Non-uniform Grids Using the Fast Fourier Transform

A. B. CAIN

Department of Aerospace and Mechanical Engineering, University of Notre Dame, Notre Dame, Indiana 46556

AND

J. H. FERZIGER AND W. C. REYNOLDS

Department of Mechanical Engineering, Stanford University, Stanford, California 94305

Received September 13, 1983

Discrete orthogonal function expansions are obtained for non-uniformly spaced data by combined use of mapping functions and the fast Fourier transform. The result yields alias-free differentiation and integration operators. The method is applicable to periodic, zero, or zero derivative boundary conditions (or combinations thereof). Truncation is required to avoid aliasing and/or singularity but the truncation error is explicit, quantitatively expressible, and generally small. This approach is demonstrated in an infinite physical domain with application to linear convection and diffusion. The resulting errors are orders of magnitude smaller than those generated by standard finite-difference methods. Difficulties arising from image fields are an important phenomena. The method of differentiation, as well as the boundary conditions, imply (artificial) image fields. A vortex-pairing problem is presented which shows that image flows can totally alter the solution. The new scheme avoids this undesirable effect by keeping image flows infinitely far away.

1. INTRODUCTION

The present work is motivated by the need for accurate numerical differentiation and integration schemes for mixed initial-boundary value problems in which the boundary conditions are imposed far from the region of physical interest.

Discrete orthogonal function expansions provide maximum accuracy for a given number of grid points. Unfortunately there are only a few orthogonal function expansions for which fast algorithms are available.

Gottlieb and Orszag [1] discuss the presently known techniques. Discrete Fourier and Chebychev expansions are the only commonly used orthogonal expansions for large problems; however, Leonard and Wray [2] recently found a particular set of Jacobi polynomials which is advantageous for the radial mode expansion of a cylin-

0021-9991/84 $3.00

drical coordinate problem. Also the Legendre polynomials are used for spherical coordinates such as in spectral weather calculations.

The most common spectral method is the discrete Fourier expansion due to Cooley and Tukey [3]. Their algorithm, the FFT (Fast Fourier Transform), reduces the number of operations from order N^2 to order $N \log N$. The original Cooley–Tukey algorithm is limited to uniformly spaced data. Winograd [4] developed an FFT which allows even more efficient expansion of certain sizes of data sets.

Application of the FFT requires uniformly spaced data in a finite domain and implies that the data are periodic. For data which vary smoothly and for which periodicity is justified, the coefficients of the resulting expansion decay rapidly. In this case a very smooth interpolation of the given data is obtained from the Fourier expansion by choosing the set of wavenumbers with minimum maximum magnitude. This smooth, continuous analytical representation of the data may be differentiated or integrated[1] with great accuracy.

If periodicity is not justified, or there are sudden jumps in the data, the Fourier expansion coefficients do not decay rapidly (if at all). In this case, the interpolation is not smooth and some other representation may be more appropriate. When the problem is due to invalid use of periodic boundary conditions, one may, in some cases, overcome the difficulty by analytic continuation. The easiest such cases are zero or zero derivative boundary conditions which may be made periodic in a larger domain by analytic continuation of a sine or cosine series. The coefficients of the resulting analytically continued periodic representation can be computed by an FFT with two or four times as many points as the physical region contains.

The use of the discrete Fourier expansion may be extended further by using polynomials to remove the non-periodic character of the data; the remaining portion of data is then expanded in the usual fashion.

Often in physical problems most of the variation in the quantity of interest occurs primarily in one or two local regions. For this class of problems *direct* use of the discrete Fourier transform is inappropriate as most of the points are effectively wasted. Mapping functions may be useful in such cases. The present work shows that there are particular mappings which, when combined with the FFT, provide a powerful method of differentiating or integrating discrete data in infinite domains. The development of the method and a few applications of physical interest are given in the remainder of this paper.

2. Standard Fourier Methods

The discrete Fourier transform is defined for any number of grid points; however, efficient algorithms usually limit the number of points to particular integers. In the most popular routines (due to Cooley and Tukey), this number is often a power of two; the Winograd [4] method allows the number of points to be the product of any

[1] There is a difficulty with an even number of data points which is addressed in the next section.

set of "mutually prime" numbers (no element of which needs to be prime). Silverman [5] demonstrates the reduction in speed of the Winograd algorithm over the Cooley–Tukey method. Since the Winograd method has not yet seen extensive application, only even numbers of data points are considered. For an odd number of data points the approach to differentiating and mapping are even simpler and directly follow the methodology below.

For a function defined on a set of uniformly spaced grid points, say, $x_n = (n-1)/N$ $(n = 1, 2, 3,..., N)$, the discrete Fourier transform can be defined by

$$\hat{f}_k = \sum_{n=1}^{N} f(x_n)\, e^{-ik2\pi x_n}. \tag{1}$$

In Cooley–Tukey algorithms $N = 2^m$ $(m = 1, 2, 3,...)$. There are an infinite number of possible choices for the wavenumbers k used in Eq. (1). As long as one is only interested in representing the function on the grid points, the choice among permissible sets is irrelevant. However, using the fast Fourier transform (FFT) as a means of obtaining derivatives or integrals implies considering Eq. (1) as an interpolation, and it is important to choose the wavenumbers which give the smoothest interpolation possible. For an even number of grid points, there are two equally good choices:

$$k = -\frac{N}{2}, \quad -\frac{N}{2}+1,..., \frac{N}{2}-1$$

or

$$k = -\frac{N}{2}+1, \quad -\frac{N}{2}+2,..., \frac{N}{2}.$$

Either choice means that the wavenumber $|k| = N/2$ is represented only by a single waveform; all other wavenumbers have two waveforms corresponding to $\pm k$. As a result, the information about the highest wavenumber component is incomplete; in fact, neither its phase nor its amplitude is known. Consequently, it cannot be differentiated or integrated. Most workers set the amplitude of the $|k| = N/2$ waveform to zero. (This problem does not occur with odd point transforms.) Using the first wavenumber set above, the derivative is

$$\left.\frac{df}{dx}\right|_{x_n} = \frac{1}{N} \sum_{k=-N/2}^{N/2-1} 2\pi i k' \hat{f}_k e^{ik2\pi x_n} \tag{2}$$

where

$$k' = k, \qquad |k| \neq N/2$$
$$k' = 0, \qquad |k| = N/2.$$

Note that in this standard application of the discrete Fourier method, the kth transform coefficient for the derivative depends only on the kth transform coefficient of the function itself. That is, in the standard Fourier method there is no coupling of modes under differentiation or integration. This is not true of the Chebychev polynomials, for which the physical data are non-uniformly spaced. In the next section a general analysis of mapping function shows that non-uniform mappings always result in modal coupling under differentiation, and, consequently, under integration.

3. Fourier Transforms on Non-Uniform Grids

Mappings are commonly used to modify the geometry such that the function is smoother in the transformed coordinate system. One can then space the mesh points uniformly in the new coordinate system. Although mappings complicate the equations to be solved, numerical methods are both more easily applied and more accurate in the transformed coordinate system. These advantages almost always outweigh the disadvantages, and coordinate transformations are a standard part of numerical methods today. Indeed, the development of better mapping methods is a major field of research.

For reasons of simplicity, attention is restricted to one-dimensional problems. Let z be the physical coordinate; and let the computational coordinate ζ be introduced through a mapping

$$z = h(\zeta). \tag{3}$$

The derivatives in the two coordinate systems are related via the chain rule:

$$\frac{df}{dz} = \frac{df}{d\zeta}\frac{d\zeta}{dz} = \frac{1}{h'}\frac{df}{d\zeta}. \tag{4}$$

In the transformed coordinate system, the function can be defined in terms of its values on a uniformly spaced grid $\zeta_j = j\,\Delta\zeta$ and can be represented as a discrete Fourier transform:

$$f(\zeta_j) = \frac{1}{N}\sum_{k=-N/2}^{N/2-1} \hat{f}_k e^{ik2\pi\zeta_j}. \tag{5}$$

The Fourier representation (5) can be used to compute the derivative $df/d\zeta$ that appears in Eq. (4). One can then multiply by the mapping metric $1/h'$ to compute df/dz as did Grosch and Orszag [6] with algebraic mappings and Chebychev expansions. The difficulties with this approach are that, in general, the result contains considerable aliasing or truncation error, and the resulting operator cannot be inverted if the number of points used is even. A more careful examination of these difficulties proves useful.

Note that $1/h'(\zeta)$, the metric which appears in Eq. (4), can itself be represented as a discrete Fourier series similar to the one in Eq. (5). In general, N terms are needed and, when this series is multiplied by the one representing $df/d\zeta$, the result contains $2N-1$ wavenumbers, $-N,\ldots, N-2$. Truncating the result to N terms produces the large truncation error alluded to above. Performing the multiplication in physical space would produce equally damaging aliasing errors.

These errors are greatly reduced by restricting the allowed mapping functions to those which contain only a few Fourier modes with small wavenumbers. Thus, suppose

$$\frac{1}{h'(\zeta)} = \sum_{k=-m}^{m} \hat{a}_k e^{ik2\pi\zeta}, \qquad m \ll \frac{N}{2}. \tag{6}$$

When this is substituted into Eq. (4), the result contains $N+2m-1$ wavenumbers. By making m small and truncating the modes whose wavenumbers are less than $-N/2+1$ or greater than $N/2-1$, a small but acceptable truncation error results provided the Fourier coefficients of f decay sufficiently rapidly. The multiplication of $1/h'$ and $df/d\zeta$ must be carried out in Fourier space with $df/d\zeta$ given by Eq. (2). If the product is taken in configuration space, the result will be aliased and the $\pm N/2$ mode will be populated making the inverse of the differentiation operator singular because $k'=0$ for $k=\pm N/2$. Defining the derivative via the truncated transform-space product allows construction of an integral operator which is the exact inverse of the differentiation operator in the sense that the derivative of the integral of f is *exactly* f provided f is defined exactly by no more than $(N-1)$ Fourier modes. These operators are alias-free in the sense that the operator itself introduces no aliasing.

We shall illustrate these ideas with two mappings suitable for free shear layer problems in fluid mechanics which are best treated in infinite domains. For plane jet or wake flows, the region of interest is infinite in the gradient direction, the boundary values are identical at $\pm\infty$, and clustering of the grid points near the origin is desirable. The cotangent provides a suitable mapping function for this case, i.e.,

$$z = h(\zeta) = -b\,\mathrm{cotan}(\pi\zeta), \qquad 0 \leqslant \zeta < 1, \quad -\infty \leqslant z < \infty. \tag{7}$$

This gives the metric

$$\frac{1}{h'} = \frac{1}{\pi b}\sin^2(\pi\zeta) = \frac{1}{2\pi b}\left[1 - \frac{(e^{i2\pi\zeta} + e^{-i2\pi\zeta})}{2}\right]. \tag{8}$$

Recalling Eq. (6), we see that $m=1$ and the Fourier coefficients of the metric are

$$\hat{a}_1 = \hat{a}_{-1} = -\frac{1}{4\pi b}, \qquad \hat{a}_0 = \frac{1}{2\pi b}. \tag{9}$$

This achieves both grid clustering near the origin and a minimum truncation error since $m = 1$. An estimate of the error in the derivative of $f(z)$ is

$$\varepsilon \simeq \frac{2}{N} \left| 2\pi \left(\frac{N}{2} - 1 \right) \hat{a}_1 \hat{f}_{N/2-1} \right| \tag{10}$$

which will be small if $\hat{f}_{N/2-1}$ is small. The mapping above is applied to a vortex-pairing problem (discussed in a later section).

Another problem of interest is the time-developing free shear layer. The major difference between this case and the previous one is that the boundary conditions are no-stress rather than periodic. A variation of the mapping (7) that is suitable for this case is

$$z = h(\zeta) = -b \operatorname{cotan}(2\pi\zeta), \qquad 0 \leqslant \zeta \leqslant \tfrac{1}{2}, \quad -\infty \leqslant z \leqslant \infty. \tag{11}$$

As indicated, the domain $0 \leqslant \zeta \leqslant \frac{1}{2}$ is the image of the physical region $-\infty \leqslant z \leqslant \infty$ under this mapping. However, the boundary conditions are such that the problem is not periodic in this domain. We can construct a periodic problem, however, by letting ζ range from zero to unity in the computation and defining the solution for $\frac{1}{2} \leqslant \zeta \leqslant 1$ by reflection about $\zeta = \frac{1}{2}$. This means that in z-space two Riemann sheets are considered, one physical, one fictitious. This method is equivalent to using a Fourier sine or cosine expansion in place of an exponential Fourier transform and twice the work is required (other special methods do not require this extra work). The choice of sine or cosine transform depends on the nature of the function being expanded. The metric resulting from this mapping is

$$\frac{1}{h'} = \frac{1}{2\pi b} \sin^2(2\pi\zeta) = \frac{1}{4\pi b} \left[1 - \frac{(e^{i2(2\pi\zeta)} + e^{-i2(2\pi\zeta)})}{2} \right] \tag{12}$$

and its Fourier coefficients are

$$\hat{a}_2 = \hat{a}_{-2} = \frac{-1}{8\pi b}, \qquad \hat{a}_{-1} = \hat{a}_1 = 0, \qquad \hat{a}_0 = \frac{1}{4\pi b}. \tag{13}$$

An estimate for the maximum error in the derivative of f in this case is

$$\varepsilon \simeq 2\pi \, |\hat{a}_2| [|\hat{f}_{N/2-1}| + |\hat{f}_{N/2-2}|] \tag{14}$$

and is small if $\hat{f}_{N/2} - 1$ and $\hat{f}_{N/2} - 2$ are small.

4. Solution of Differential Equations

When solving differential equations numerically it is important (and often essential) that the integral and differential operators be exact inverses of each other. Such consistent operators may be defined by using the results of the previous section.

For the sake of definiteness, let us consider mapping (7). The method of the preceding section gives

$$\left.\frac{\delta f}{\delta z}\right|_{z_j} = \frac{1}{Nb} \sum_{k=-N/2+1}^{N/2-1}{}' \left[ik\hat{f}_k - \frac{i(k-1)}{2}\hat{f}_{k-1} - \frac{i(k+1)}{2}\hat{f}_{k+1} \right] e^{ik2\pi\zeta_j} \tag{15}$$

where the prime on the summation indicates that any term with an index of magnitude greater than $(N/2-1)$ is zero. Similarly, the second derivative is

$$\begin{aligned}\left.\frac{\delta^2 f}{\delta z^2}\right|_{z_j} = \frac{1}{Nb} \sum_{k=-N/2+1}^{N/2-1}{}' \Bigg\{ & \frac{ik}{b}\left[ik\hat{f}_k - \frac{i(k-1)}{2}\hat{f}_{k-1} - \frac{i(k+1)}{2}\hat{f}_{k+1} \right] \\ & \frac{-i(k-1)}{2b}\left[i(k-1)\hat{f}_{k-1} - \frac{i(k-2)}{2}\hat{f}_{k-2} - \frac{ik}{2}\hat{f}_k \right] \\ & \frac{-i(k+1)}{2b}\left[i(k+1)\hat{f}_{k+1} - \frac{ik}{2}\hat{f}_k - \frac{i(k+2)}{2}\hat{f}_{k+2} \right] \Bigg\} e^{ik2\pi\zeta_j}. \end{aligned} \tag{16}$$

Similar application to the no-stress mapping (11) gives

$$\left.\frac{\delta f}{\delta z}\right|_{z_j} = \frac{1}{2bN} \sum_{k=-N/2+1}^{N/2-1}{}' \left[ik\hat{f}_k - \frac{i(k-2)}{2}\hat{f}_{k-2} - \frac{i(k+2)}{2}\hat{f}_{k+2} \right] e^{i2\pi k\zeta_j} \tag{17}$$

and

$$\begin{aligned}\left.\frac{\delta^2 f}{\delta z^2}\right|_{z_j} = \frac{1}{2bN} \sum_{k=-N/2+1}^{N/2-1}{}' \Bigg\{ & \frac{ik}{2b}\left[ik\hat{f}_k - \frac{i(k-2)}{2}\hat{f}_{k-2} - \frac{i(k+2)}{2}\hat{f}_{k+2} \right] \\ & - \frac{i(k+2)}{4b}\left[i(k-2)\hat{f}_{k-2} - \frac{i(k-4)}{2}\hat{f}_{k-4} - \frac{ik}{2}\hat{f}_k \right] \\ & - \frac{i(k+2)}{4b}\left[i(k+2)\hat{f}_{k+2} - \frac{ik}{2}\hat{f}_k - \frac{i(k+4)}{2}\hat{f}_{k+4} \right] \Bigg\} e^{i2\pi k\zeta_j}. \end{aligned} \tag{18}$$

To illustrate this method, consider the solution of a typical elliptic problem, that of solving the Poisson equation

$$\nabla^2 P = Q. \tag{19}$$

This equation may be solved by use of the three-dimensional Fourier transform. The solution is very easily and accurately obtained for the periodic case on a finite domain with a uniform grid in all three directions. The Fourier coefficients of P are obtained by dividing $\hat{Q}(\mathbf{k})$ by the negative of the square of the magnitude of the wavenumber vector $|\mathbf{k}|$. P is then found by the discrete Fourier inversion. This process can be expressed in terms of the linear algebraic system for the Fourier coefficients as

$$A[\hat{P}] = [\hat{Q}]. \tag{20}$$

In the above case, A is a diagonal matrix. It is also singular with a one-parameter family of solutions to the homogeneous equation due to the $k_1 = k_2 = k = 0$ mode ($\hat{P}(\mathbf{0})$) which is an undetermined constant. Thus $P = P_p + c$ where c is an undetermined constant and P_p is a particular solution. This constant is a solution to the homogeneous equation which satisfies the periodic boundary conditions. In most physical problems only the derivative of the solution is important and this constant may be set to zero without loss of information.

The situation with a non-uniform grid in one of the three coordinate directions is only slightly more involved. Let x_1 and x_2 be uniform grid directions with corresponding wavespace components k_1 and k_2. A three-dimensional wavespace is now defined by the third orthogonal component k, from the transformed uniformly mapped coordinate ζ. The non-zero matrix coefficients for mapping (7) are

$$\begin{aligned}
a_{k,k-2} &= -\frac{(k-1)(k-2)}{4b^2} \\
a_{k,k-1} &= \frac{k(k-1)}{2b^2} + \frac{(k-1)^2}{2b^2} \\
a_{k,k} &= -k_1^2 - k_2^2 - \frac{k^2}{b^2} - \frac{k(k-1)}{4b^2} - \frac{k(k+1)}{4b^2} \\
a_{k,k+1} &= \frac{k(k+1)}{2b^2} + \frac{(k+1)^2}{2b^2} \\
a_{k,k+2} &= -\frac{(k+1)(k+2)}{4b^2}.
\end{aligned} \tag{21}$$

Mapping (11) gives

$$\begin{aligned}
a_{k,k-4} &= -\frac{(k-2)(k-4)}{16b^2} \\
a_{k,k-2} &= \frac{k(k-2)}{8b^2} + \frac{(k-2)^2}{8b^2} \\
a_{k,k} &= -k_1^2 - k_2^2 - \frac{k^2}{4b^2} - \frac{k(k-2)}{16b^2} - \frac{k(k+2)}{16b^2} \\
a_{k,k+2} &= \frac{k(k+2)}{8b^2} + \frac{(k+2)^2}{8b^2} \\
a_{k,k+4} &= -\frac{(k+2)(k+4)}{16b^2}.
\end{aligned} \tag{22}$$

In expressions (21) and (22) any parenthetic factor of magnitude greater than $(N/2 - 1)$ is set to zero. The first matrix element subscript runs vertically and

corresponds to row k and mode k; the second subscript corresponds to the column position. The resulting matrix systems are non-singular[2] and are readily solved by standard techniques. Obviously if a function is integrated in this way and then differentiated the original function is recovered.

Thus finding the full set of $\hat{P}$ requires the solution of $[(N_1 - 1)(N_2 - 1)]$ systems of $(N-1) \times (N-1)$ pentadiagonal matrix equations. For real data, only half as many systems need to be solved as $\hat{P} - (\mathbf{k}) = \hat{P}^*(\mathbf{k})$ where the asterisk denotes the complex conjugate. The matrix for $k_1 = k_2 = 0$ is singular (rank $N-2$) and only the equations for $k = 1, 2, 3, \ldots, N/2 - 1$ are solved using $\hat{P}(k=0) = 0$ and $\hat{P}(-k) = \hat{P}^*(k)$.

The basis for discrete orthogonal function expansions for derivative and integral operators is now defined through use of the fast Fourier expansion and a restricted set of mapping functions. The formulation is conveniently expressed in terms of linear algebraic equations for the Fourier coefficients. The non-uniform grid is shown to result in a coupling of the transform coefficients. This coupling results in a centered tridiagonal matrix operator for the Fourier coefficients of the first derivative, and a pentadiagonal one for the second. The infinite domain may be used in more than one direction but the subsequent solution of the Poisson equation would require inversion of a very large matrix or use of an ADI- or SOR-type approach.

5. Application to Test Problems

In this section, three problems are solved using the method defined above. Comparison with analytical and finite-difference solutions are appropriate for the first two problems. The third problem demonstrates one of the major reasons for development of this method.

A. *Convection*

Mapping (11) is evaluated here but the results apply to both mappings. The one-dimensional convection equation is

$$\frac{\partial u}{\partial t} + c\frac{\partial u}{\partial z} = 0 \tag{23}$$

and has the exact solution

$$u(z, t) = f(z - ct) \tag{24}$$

which says that any initial waveform propagates toward increasing z with uniform speed c. A Gaussian initial condition is used, for which the exact solution to Eq. (23) is

$$u(z, t) = \exp\{-[1.6651(z - ct)/\delta_{1/2}]^2\}.$$

[2] Recall that the values of k are $k = -N/2 + 1, -N/2 + 2, \ldots, N/2 - 1$.

In the problem solved, $\delta_{1/2} = 4$ and $c = -1$; $\delta_{1/2}$ is the width of the waveform at half its peak value.

Using mapping (11), which is appropriate for functions which vanish or whose derivatives vanish at ±infinity, we fixed the grid by using $b = 32/\pi$ and 33 physical points. Although one can use the complex exponential transform in this problem, a combination of sine and cosine transforms were used.

Another way of looking at this is to use the Riemann sheet perspective. A cosine expansion implies a function imaged symmetrically about infinity onto a second Riemann sheet. Similarly, a sine expansion implies an antisymmetric reflection onto the second Riemann sheet. The physical and image solutions will propagate toward one another and meet at infinity at infinite time. The combination

$$\frac{\delta u}{\delta z} = \frac{1}{2}\left[\left.\frac{\delta u}{\delta z}\right|_{\sin} + \left.\frac{\delta u}{\delta z}\right|_{\cos}\right]$$

produces no image on adjacent Riemann sheets, and periodicity is obtained over two Riemann sheets. All solutions are identical and propagate with equal speed in the same direction.

The time integration is accomplished by the well-known fourth-order Runge–Kutta scheme with Courant number $\Delta t\,|c|/\Delta z_{\min} = 0.01$. The time step was chosen small so that the error is dominated by that of the spatial-differencing scheme.

We also solved this problem using two common finite-difference schemes on the same non-uniform grid. The first is

$$\left.\frac{\delta u}{\delta z}\right|_{z_j} = \alpha u_{j-1} + \beta u_j + \gamma u_{j+1} \tag{25}$$

where

$$\alpha = -\frac{1}{(\Delta_{j-1}^2/\Delta_j) + \Delta_{j-1}}, \qquad \gamma = \frac{1}{\Delta_j + (\Delta_j^2/\Delta_{j-1})}$$

$$\beta = -\alpha - \gamma$$

$$\Delta_j = z_{j+1} - z_j$$

and the second is

$$\left.\frac{\delta u}{\delta z}\right|_{z_j} = \alpha u_{j-1} + \gamma u_{j+1}$$

$$\alpha = -\gamma = -\frac{1}{z_{j+1} - z_{j-1}}. \tag{26}$$

The scheme given by Eq. (25) is second order in physical space and slightly more accurate than Eq. (26), which is second order in computational space but first order in physical space.

Figure 1 shows the exact solution and the computed solutions at $T = ct/\delta_{1/2} = 2.0$ obtained using Eq. (25) and the new Fourier scheme. The maximum error in the solution is 0.34 using Eq. (25), 0.40 using Eq. (26), and 0.0032 for the new Fourier scheme. Thus the new Fourier method is superior to finite-difference calculation for this problem.

B. *Diffusion*

Now consider a diffusion problem.

$$\frac{\partial u}{\partial t} = \nu \frac{\partial^2 u}{\partial z^2} \tag{27}$$

is solved using the same grid as for the convection problem.

The fourth-order Runge–Kutta scheme was used for the time advance with a dimensionless time step

$$\frac{\nu \Delta t}{\Delta z^2_{\min}} = 0.05625.$$

Two finite-difference schemes for the second partial derivative were used. The first scheme is two consecutive applications of (25); the second finite-difference scheme is given by

$$\left.\frac{\delta^2 u}{\delta z^2}\right|_{z_j} = \alpha u_{j-1} + \beta u_j + \gamma u_{j+1} \tag{28}$$

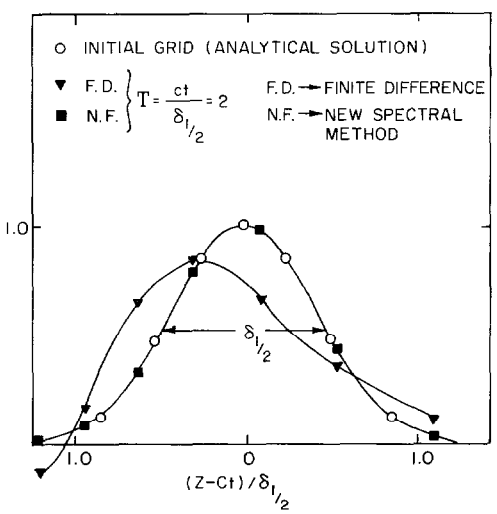

FIG. 1. Comparison of finite-difference, new Fourier, and analytical solutions to the first-order convection equation.

where

$$\alpha = 2/[\Delta_{j-1}(\Delta_j + \Delta_{j-1})]$$
$$\beta = -2/\Delta_j\Delta_{j-1}$$
$$\gamma = 2/[\Delta_j(\Delta_j + \Delta_{j-1})].$$

Representation (28) is a three-point scheme and is first-order accurate; it becomes second order as $\Delta_{j-1} \to \Delta_j$.

The initial condition used was an error function, giving the self-similar analytical solution:

$$u(z, t) = \operatorname{erf}[z/\sqrt{4vt}\,].$$

The computations were begun at $t_0 = 25$ and the computation was advanced until $t_f = 16t_0$; v was 0.06.

Figure 2 shows the time history of the maximum normalized error defined by

$$E_m = \frac{(u_c - u_A)_{max}}{(u_0 - u_A)_{max}}$$

as a function of dimensionless time, where $u_0 = u(x, t = 0)$, u_A is the analytical solution, and u_c is the computed solution. The new Fourier scheme has errors six

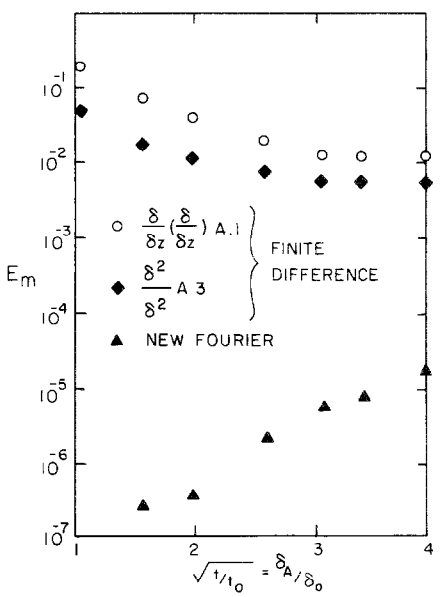

FIG. 2. Comparison of the maximum dimensionless errors of finite-difference and new Fourier solutions to the heat or diffusion equation.

orders of magnitude smaller than the finite-difference method at early times and three orders of magnitude smaller at later times. Thus the new Fourier method is also far superior to the finite-difference method for this problem.

C. *Vortex Interactions*

Boundary conditions meant to be applied at infinity are often applied at a finite location. When this is done, the boundary conditions imply unphysical image solutions which can cause errors. In severe cases, interaction of the image solutions and the physical one may render the computed solution meaningless. The new Fourier method puts the image flows infinitely far away, thus eliminating this difficulty. Couet and Leonard [7] used analytical extension of the boundary conditions at infinity to some finite location as an alternative solution to this problem.

Suppose one wishes to compute the flow due to two vortices of the same sign. One method to apply a no-stress boundary condition at a finite distance from the vortices is to use discrete sine and cosine transforms. This implies an infinite array of pairs of image vortices with alternating signs of vorticity. In order to assess how much the image flows affect the computed solution, the following numerical experiment is performed. First two pairs of vortices of opposite sign are placed a distance $d/2$ above and below the x axis, respectively, as shown in Fig. 3. The vortices have elliptical Gaussian distributions of vorticity with eccentricity $\frac{3}{4}$ and separation distance c. If $d \gg c$, the upper vortices rotate about one another in a clockwise manner, while the lower pair rotate counterclockwise. Furthermore, if the pairs are far enough apart not to affect one another, a horizontal shift in the location of the lower pair of vortices by a distance $c/2$ should give identical results. In this calculation, the mapping given Eq. (7) was used. The standard Fourier method for differentiating in the x-direction and the second-order Adams–Bashforth scheme was employed for the time advance.

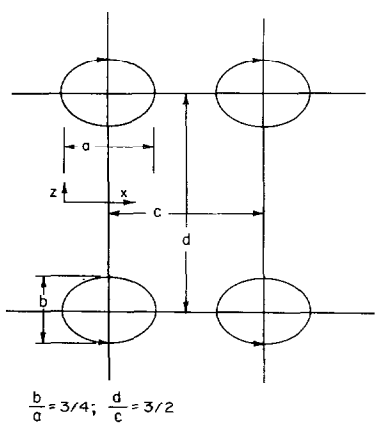

FIG. 3. Schematic view of vortex pairing, image flow study.

The grid had 16 points in the x-direction and 128 in the z-direction. The vortex pairs were centered at grid points 59 and 71 in z and grid points 5 and 11 in x. The coefficient b, of the mapping function, was $b = 192\pi$ (this gives $\Delta z = 1.5$ near the origin); the dimensionless time step was selected so that $(u_{\max}/\Delta x + w_{\max}/\Delta z_{\min})\,\Delta t = 0.3$. This problem was solved using the vorticity equation

$$\frac{\partial}{\partial t}\omega + \frac{\partial}{\partial x}u\omega + \frac{\partial}{\partial z}w\omega = \nu\nabla^2\omega \tag{29}$$

and the vector potential equation

$$\nabla^2\psi = -\omega. \tag{30}$$

Since the vorticity equation is non-linear the calculation was done pseudospectrally for efficiency but all aliasing is due to this real space non-linear product, not the mapping for differentiation. The velocity components are obtained from

$$u = -\frac{\partial}{\partial z}\psi, \qquad w = \frac{\partial}{\partial x}\psi. \tag{31}$$

Integrating until dimensionless time $T = u_{\max}t/c = 1.0$, at which point we compared the "turbulent" kinetic energy (turbulence is defined as the local deviation from the x-direction) average with the initial "turbulent" energy. For the case shown in Fig. 3, the turbulent kinetic energy was the same at $T = 1$ and $T = 0$. However, when the lower pair of vortices was shifted by $c/2$, the turbulent kinetic energy at $T = 1$ was double the turbulent energy at $T = 0$.

One thus concludes that a computation with $d/c = 1.5$ suffers tremendously from the influence of image flows. The same calculation performed with $d/c = 4$ shows no significant image flow influence.

Conclusion

A technique for applying discrete Fourier series to infinite domains has been presented. It makes use of mappings designed to minimize truncation error and can be applied to the solution of mixed initial boundary value problems among others. The method is alias-free, and yields consistent differentiation and integration operators. The mapping-induced truncation error is explicitly expressible and small in nearly all cases of interest.

The differentiation operators resulting from this method are equivalent to tridiagonal matrices in Fourier space. Solution of a second-order equation requires inversion at a pentadiagonal system of equations for the Fourier coefficients. In applications of the approach to linear convection and diffusion equations the errors are orders of magnitude smaller than those generated by finite-difference techniques with equal numbers of points.

Image flow effects are demonstrated in a vortex-pairing problem. The results show the possibility of large distortions due to image flows. The present method removes the difficulty by moving image flows infinitely far away.

ACKNOWLEDGMENTS

The authors wish to gratefully acknowledge the financial and facilities support of NASA Ames Research Center, Moffett Field, California, and the comments of Drs. R. A. Howland and T. J. Akai of the University of Notre Dame concerning the presentation of this material.

REFERENCES

1. D. GOTTLIEB AND S. A. ORSZAG, "Numerical Analysis of Spectral Methods: Theory and Applications," SIAM (Monograph) Appl. Math., Philadelphia, 1977.
2. A. LEONARD AND A. WRAY, A numerical method for the simulation of three-dimensional flow in a pipe, *in* "Proceedings, International Conference on Numerical Methods in Fluid Dynamics."
3. J. W. COOLEY AND J. W. TUKEY, An algorithm for the machine calculations of complex Fourier series, *Math. Comp.* **19** (1965), 294–301.
4. S. WINOGRAD, On computing the discrete Fourier transform, *Math. Comp.* **32** (1978), 175–199.
5. H. F. SILVERMAN, An introduction to programming the Winograd Fourier transform algorithm (WFTA), *IEEE Trans. Acoust. Speech Signal Process.* **ASSP-25** (2) (1977), 152–165.
6. C. E. GROSCH AND S. A. ORSZAG, "Numerical Solution of Problems in Unbounded Regions: Coordinate Transformations," TR No. 26, Institute of Oceanography, Old Dominion University, Norfolk, Virginia, 1976.
7. B. COUET AND A. LEONARD, Exact extension to the infinite domain for the vortex-in-cell method, *SIAM J. Sci. Statist. Comput.* **2** (3) (1981), 311–320.